https://adv-j-sci-eng.com eISSN: 2717-0705

Advanced Journal of Science and Engineering

Original Research

Finite Element Analysis Assisted Improvement of Ionic Polymer Metal Composite Efficiency for Micropump of 3D Bioprinter

Amin Nasrollah[1], **Hamid Soleimanimehr**[1,✉], **Sara Javangoroh**[1]

[1] *Department of Mechanical Engineering, Science and Research Branch, Islamic Azad University, Tehran, Iran*

✉ *Corresponding author*: **H. Soleimanimehr**; *E-mail address*: **soleimanimehr@srbiau.ac.ir**, *ORCiD*: **0000-0001-8931-5698**.

Received: 17 December 2020 / ***Accepted***: 08 March 2021 / ***Published Online***: 30 March 2021

ABSTRACT

Nowadays, smart materials for manufacturing bioprinters have diverse usages; micropump is one other product resulted by using smart materials such as IPMC, piezo, and etc., in manufacturing above mentioned printers. This item has an important role in micro systems and delivering special fluid such as nanofluids. In order to manufacture this type of pump a wide range of materials can be used. In this research, a smart material named ionic-polymer-metal composite (IPMC) is used; however, the current material for them is piezoelectrics. IPMC systems are mostly used in micro pump diagrams because of their self-assessment feature, low starting voltage, and elastic structure. In order to increase the IPMC actuator's durability and also enlarging the deformation range, a new design for IPMC diaphragms is introduced in this paper. In prevalent designs, all the actuator edges where clamped, but here different IPMC actuators in circular and triangular shapes are presented. And also the new design allows the solvent to completely cover the diaphragm by separating the fluid from IPMC. IPMC strain and stresses are modeled in order to analyze the efficiency of the new design. The results show that the presented designed IPMC works steadily for a longer duration of time. It also has a wider deformation range and more efficiency compared to the conventional design.

KEYWORDS Bioprinter, Micropump, IPMC, Piezoelectric, Finite element analysis.

CITE Nasrollah A, Soleimanimehr H, Javangoroh S. Finite Element Analysis Assisted Improvement of Ionic Polymer Metal Composite Efficiency for Micropump of 3D Bioprinter. Advanced Journal of Science and Engineering. 2021;2(1):23-30.

DOI https://doi.org/10.22034/advjscieng21021023

URL https://sciengpub.com/adv-j-sci-eng/article/view/advjscieng21021023

INTRODUCTION

If an organ failed in body, scientists are forced to harvest cells or create implants, it should be mentioned that the above-mentioned items require a specific method.[1] Printing cells with 3D printers is a common way to accomplish this goal. The cell printing method has solved many of human complicities by the exploitation of biology and biomedical engineering. Nowadays microsystems have a great potential to be used for different proposes such as medical transformations, micro cooling systems.[2] Producing 3D live fabrics consists of different processes. Briefly, building a basic construction called scaffold and then placing cells and multiplying them are the most important stages and stimulation mechanisms used in micro-pumps for 3D printers are piezoelectric, magnetic, electrohydrodynamic, and magneto-hydro-dynamic.[3] Using diaphragm is a conventional method for making a dynamic pump. In these pumps, the diaphragm vibrates periodically and this vibration causes volumetric changes in the pump. Nowadays, usage of smart materials is literally extended; smart materials are sensitive to specific stimulation. With enhancing their structure enormous properties will appear in them.[4] Piezoelectrics are the most

important smart material used in our world. Piezoelectrics have many applications and due to their fast response and large output force are the most common material used in diaphragm pumps.[5, 6] Other stimulus mechanisms used in micropumps are electromagnetic, pneumatic, shape memory alloys, etc. Ionic polymer-metal composites (IPMC) have recently been introduced as stimulus material for some biomechanical systems.[7] They are one of the best choices for micro pump diaphragms because of their low working voltage, high deformation capacity, and self-assessment feature.[8] Fig. 1 shows an IPMC micro pump diaphragm. In this sample, the diaphragm is clamped at all edges and the voltage alteration causes deformation and volumetric changes. Although IPMC is commonly used in the micropumps, they have some disadvantages such as clamping all the edges which may decrease the deformation ability, the short working duration, and the fact that IPMC diaphragm's efficiency lowers due to the electrolysis and the ionic concentration.[9] By lessening the edge constrains some of the problems mentioned can be solved and also using ionic liquids as pumping fluid can decrease the possibility of electrolyzeation.[10]

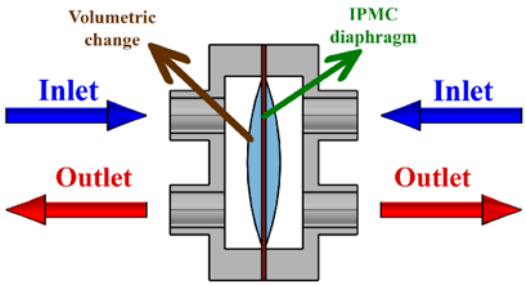

Fig. 1: Diaphragm of a conventional IPMC micropump.

In this paper, a new method for designing IPMC diaphragm actuators is introduced in which the actuator is covered by two thin elastic layers. Our goal is to increase efficiency, deformation ability, and working duration of the IPMC diaphragm actuator.[11] First, the implicit differential equations, defining the IPMC actuator are derived and the stress and the strain of the IPMC are analyzed by a CAE software, named Abaqus.[12] These stresses and strains are added to the model by the finite element method. In the new design, the IPMC actuators are symmetric and each is clamped at separate edges. This technique decreases constrains and increases deformation ability and also two thin layers separate the fluid from the actuator. Our analysis results claim that the triangular actuator has the most efficiency. Indeed, computer-based research works could provide insightful information for various systems.[13-15] Here the analyses in three different ways are examined, deformation vs. input voltage, deformation vs. input frequency and durability, and strength. Results show that the new design responds to 5 V and 0.05 Hz sinusoidal voltage by 0.4 mm deformation and the steady-state working duration is 35 min at the same time the conventionally designed actuator responses to the same frequency and voltage by 0.2 mm deformation and 8 min working durability. In this paper, the new and more efficient design and the related analyses by Abaqus are explained.

MATERIALS & METHODS

Simulation for the IPMC Actuator Stress Pattern

In this section, the IPMC actuator is analyzed under a certain voltage. This analysis is done by evaluating the partial differential equations defining the actuator.[16] An electromechanic actuator (Fig. 2) is described by eq. (1), in which σ is stress, ρ is electric charge and α_0 is coupling constant calculated by experimental tests.[17] In this equation, α0 is coupling constant and it is calculated by experimental tests.

$$\sigma(x,y,z,t) = \alpha_0 \rho(x,y,z,t) \quad (1)$$

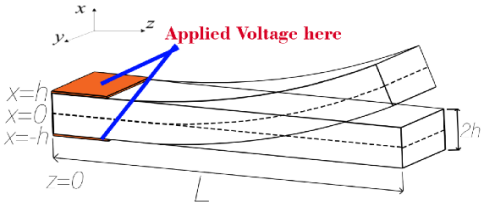

Fig. 2: Simulation for IPMC actuator.

Ionic flux vector (*J*) in the IPMC transducer can be calculated by eq. (2).[18]

$$J = -d\left(\nabla C^{+} + \frac{C^{+}F}{RT}\nabla\varphi + \frac{C^{+}\Delta V}{RT}\nabla p\right) + C^{+}v \tag{2}$$

Here *d* is the ionic diffusivity, C^{+} is the cation concentration, *F* is the Faraday constant, *R* is the ideal gas constant, *T* is the absolute temperature, *Φ* is the electric potential, *ΔV* is the volumetric change and *p* is the free velocity field. The IPMC thickness is insignificant compared to the length and width so it is neglected thus the motion only exists in the *x*-direction.

Infield equations by using Darcy's law small terms are neglected and the equation would be written as eq. (3).[19]

$$J = -d\left(\frac{\kappa}{f}\frac{\partial^2 E}{\partial x^2} - \frac{FC^{-}}{RT}(1 - C^{-}\Delta V)\right)E \tag{3}$$

Continuity of equations depends on cation concentration (C^{+}) and ionic variation vector (*J*) as indicated by eq. (4).[20]

$$\frac{\partial J}{\partial x} = -\frac{\partial C^{+}}{\partial t} \tag{4}$$

The implicit differential equation that defines the electric field is eq. (5).[11]

$$\frac{\partial}{\partial x}\left[\partial\frac{(\kappa E)}{\partial t} - d\frac{\partial^2(\kappa E)}{\partial x^2} + \frac{F^2 dC}{kRT} - (1 - C^{-}\Delta V)(kE)\right] = 0 \tag{5}$$

Or the equation can be written by using electric load density as indicated by eq. (6).[11]

$$\frac{\partial\rho}{\partial t} - d\frac{\partial^2(\rho)}{\partial x^2} + \frac{F^2 dC^{-}}{\kappa RT} - (1 - C^{-}\Delta V)\rho = 0 \tag{6}$$

C^{-} shows anion concentration and κ is the dielectric constant of the polymer. Here are the answers for eqs. (5) and (6) are explained.

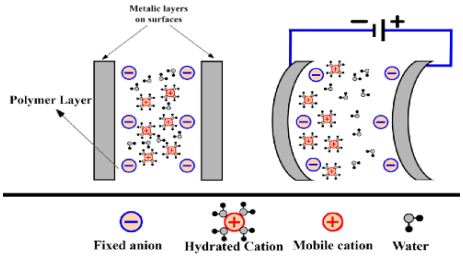

Fig. 3: Working process of IPMC actuator.

First of all, it should be noted that IPMC consists of two outer layers from noble metal as the electrode, a polymer ion membrane on each side which is made of fixed anions and moving electrons (Fig. 3). Because of the fixed anions, adding a voltage step would result in asymmetric ion division, which has been neglected in the equations above.[17] Now, the equations considering the asymmetric ionic distribution are solved. Eq. (3) can be written as eq. (5) in steady-state *J*=0 and $(\partial C^{+}/\partial x) = 0$.[10]

$$\frac{\partial^2 E}{\partial x^2} - KE = 0\ ,\quad K \triangleq \frac{F^2 C^{-}}{\kappa RT}(1 - C^{-}\Delta V) \tag{7}$$

Electric density is constant in anode boundary layer as $\rho_{(1)} = -C^{-}F$ and $\rho_{(2)} = (C^{+} - C^{-})F$ in other parts. Load density *ρ*, electric field *E*, and electric potential *Φ* in the anode boundary layer are shown below in eq. (8).[21]

$$\begin{cases} \rho_{(1)}(x) = -C^{-}F \\ E_{(1)}(x) = \dfrac{1}{\kappa}(-C^{-}Fx + E_0)\ ,\ (-h \le x \le -h + w) \\ \phi_{(1)}(x) = \dfrac{1}{\kappa}\left(\dfrac{C^{-}Fx^{2}}{2} - E_0 x\right) + A_0 \end{cases} \tag{8}$$

W is anode layer thickness. A_0 and E_0 are integration constants. For other parts, eq. (7) can be written as eq. (9).[21]

$$E_{(2)}(x) = C_1 exp(\sqrt{Kx}) + C_2 exp(-\sqrt{Kx})$$
$$\phi_{(2)}(x) = \frac{1}{\sqrt{K}}\left(-C_1 exp(\sqrt{Kx}) + C_2 exp(-\sqrt{Kx})\right) + C_3 \quad (9)$$
$$\text{،} (-h + w \leq x \nleq h)$$
$$\rho_{(2)}(x) = \kappa\sqrt{K}\left(C_1\, exp(\sqrt{Kx}) - C_2\, exp(-\sqrt{Kx})\right)$$

C_1, C_2, C_3 are integration constants. The equation describing load density in steady-state for an IPMC actuator under one step of voltage is eq. (10).[18]

$$\rho^*(X) = \begin{cases} -C^- F & \text{،} \quad (-h \leq x \leq -h + w) \\ \kappa\sqrt{K}(C_1 exp(\sqrt{K}x) - C_2 exp(-\sqrt{K}x)) \end{cases} \quad (10)$$

IPMC model parameters considering boundary conditions and neglecting surface resistance are shown in Table 1. The equation for the dynamic of a charging model is written as eq. (11).[18]

$$\rho(x,t) = \left(1 - exp\left(\frac{-t}{\tau}\right)\right)\rho^*(x)\,,\ \tau = \frac{\kappa RT}{dC - F} \quad (11)$$

τ is the estimated time required for the cation division. The electric load density throughout thickness for 1.5 V voltage is shown in Fig. 4. Considering load density distribution, it is possible to calculate inner stress σ under-voltage Φ. The stress changes throughout IPMC thickness but remains constant on the YZ plane.

Table 1: Parameters of the IPMC charging model.[16]

$F = 69.487\ C/mol$
$H = 100\ \mu m$
$C_1 = \sqrt{K}\, exp(-h\sqrt{K})\,(\varphi_0 + \frac{RT}{F}\left((exp(w-h)\sqrt{k}\right) - \frac{(w\sqrt{k}+1)^2 + 1}{2}$
$R = 8.3143\ j/mol.k$
$C_2 = \sqrt{K}\frac{RT}{F} exp((w-h)\sqrt{k})$
$T = 300\ K$
$C = 1200\ mol.m^3$
$d = 1.030 \times 10^{-10}\ m^2/s$

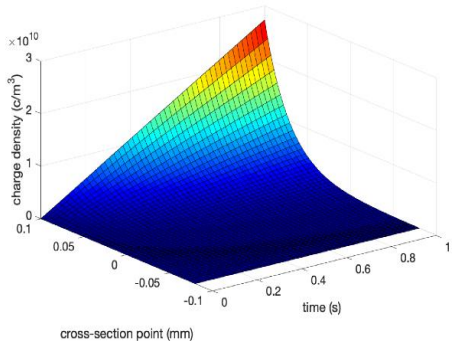

Fig. 4: Simulation for charge density profile.

Visual Simulation of the IPMC Actuator by Finite Element Method

Inner stresses cause deformation in the IPMC actuator. In order to simplify the analyses, the finite element method is used for simulating process. The inner stress σ is calculated by solving eq. (1) then the constraints at the clamped edges of the IPMC actuator are taken as boundary conditions and the deformation limit for the neutral plane is considered. A visual simulation for an IPMC actuator by 3 V constant voltage is shown in Fig. 5. The IPMC elastic modulus and Poisson's ratio are respectively 5.71 × 108 Pa and 0.48. Size of the IPMC actuator is 30 × 6 × 0.2 mm and the diaphragm radius is 0.5 mm. It is obvious that the maximum deformation for the mentioned actuator is 6.04 mm and the maximum inner strain is 0.02. In the next section, the design of an IPMC actuator is going to be explained.

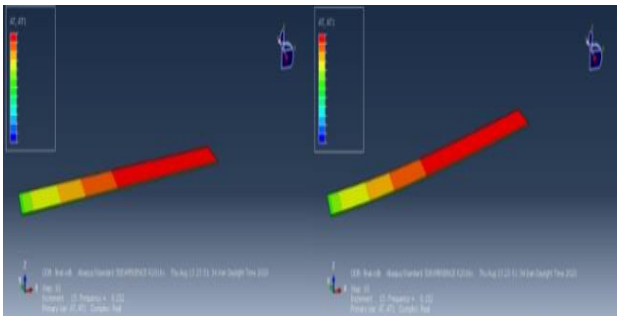

Fig. 5: Simulation for conventional IPMC actuator.

Design of an IPMC diaphragm

First, the conventional IPMC actuator will be explained and then a new and more efficient design would be introduced. In the conventional IPMC micropumps, the actuator is circular and it is clamped at all edges to form a close pumping chamber. This design prevents IPMC to have deformation at edges and also increases pumping ability.

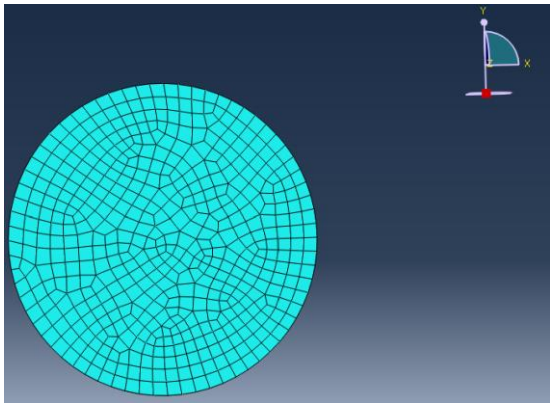

Fig. 6: Finite element model of conventional IPMC diaphragm.

Fig. 6 shows a simulation for conventional IPMC actuator under 3 V voltage, by finite element method which includes 729 elements. Deformation and inner strains are shown in Figs. 7 and 8. In this simulation, the maximum deformation is 0.15 mm and the volumetric change due to the deformation is 6.09 ml. Contrarily to the IPMC cantilever beam, the conventional IPMC actuator deformation causes higher strains. As a result of cation concentration, a part of the cathode layer bends as much as the maximum strain amount. To cancel the stress effects, the whole parts of the IPMC should bend towards cathode layer, this deformation requires a large amount of energy, and this process causes the IPMC actuators to have less deformation capacity compared to the cantilever beams.

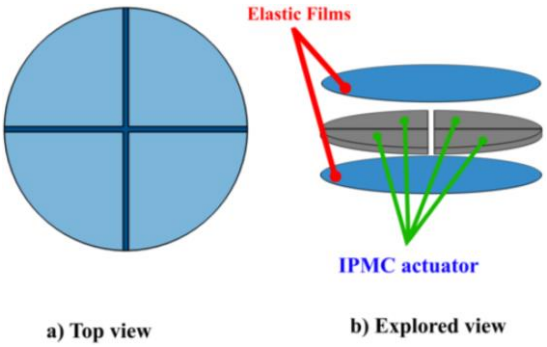

Fig. 7: Circular IPMC diaphragm.

RESULTS & DISCUSSION

The Structure Proposed for IPMC Diaphragm

In order to increase deformations, a new design is proposed, which consists of several elastic diaphragms. Fig. 7 shows a circular diaphragm consisting of four-quadrant actuators covered with two thin elastic films. In this new

structure, the boundary constraints are omitted and a part of energy loss is prevented and the deformation capability is increased. Two elastic films are made of polytetrafluoroethylene with 0.02 mm thickness and 3 ×108 Pa young modulus. Thus, these films have high deformation capability, they do not interfere with IPMC displacements. In the following, the simulation for circular IPMC diaphragm with 10 mm thickness is explained. Deformation for the mentioned diaphragm under 3 V voltage is shown in Fig. 8 and in this case, maximum deformation is 0.35 mm and volumetric change is 11.24 ml. These results show that the circular diagram is more efficient than the conventional one. In Fig. 8, the strain pattern is shown. The new diaphragm bending direction is contrary to the conventional one it means that the IPMC actuator bends toward the anode layer under the amount of voltage defined as Φ.

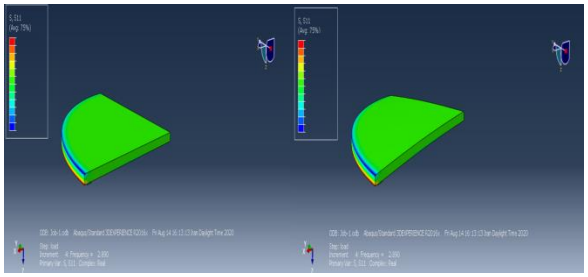

Fig. 8: Deformation and strain pattern for circular IPMC diaphragm.

The Effective Shape of Proposed IPMC Diaphragm

In order to estimate and explain the deformation ability of the proposed IPMC diaphragm, the triangular design for IPMC actuators is introduced. That has the same area as the circular one. Deformation and inner strains for triangular actuators are shown in Fig. 9. Under 3 V voltage the maximum deformation for this diaphragm are 0.42 mm and volumetric change is 16 ml. Through further analyses, it is found out that the triangular diaphragm has more deformation ability it can bear about 171 % volumetric change and 184 % deformation. The strain rate in the triangular diaphragm is less than the circular one.

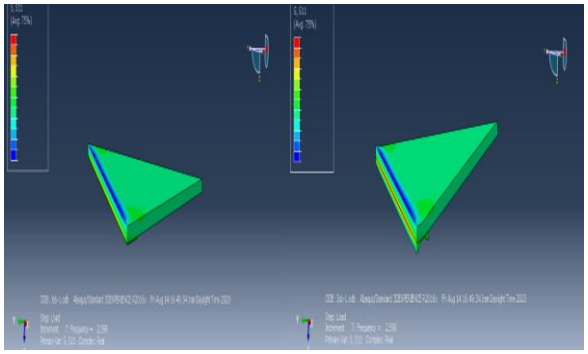

Fig. 9: Deformation and strain pattern for circular IPMC diaphragm.

While the pumping proses all the diaphragms should stretch to provide the deformation needed, in the former designs minimum deformation occurred when the maximum strain happened but in the circular design due to neglecting boundary constrains, more deformation happens alongside the maximum strain. It is clear that the triangular structure provides more deformation and volumetric change due to less strain. As the triangular IPMC design has more efficiency it is used in experimental tests

Testing System Setup

In this section the system required for examining the triangular diaphragm is going to be explained which consists of four actuators and the voltage is applied to the electrode so the bending would occur. Two thin PTFE films cover the actuators and form a close pumping section. The simulating procedure is done by MATLAB. Two multi-function data acquisition Advantech cards, A/D 1711 and D/A 1720, are added to the system and a Laser displacement sensor is also used in order to measure the deformation of the central point of the diaphragm. The bending behavior of the diaphragm is measured by the voltage applied to IPMC. The input signal is sent from the processing system through the 1720 D/A converter.

Deformation under the Input Voltage

To analyze the diaphragm, structure the deformation under different voltages, from 0 V up to 5 V is captured. Fig. 10 shows the diagrams for the deformation of triangular diaphragm compared to circular and conventional forms. It is clear that circular and triangular IPMCs have more deformation capacity. The results are reliable for low voltages (under 3V) but in higher voltages, the experimental results indicate less deformation. This may be a result of neglecting the nonlinear parts of the implicit equations of other research.[20,22]

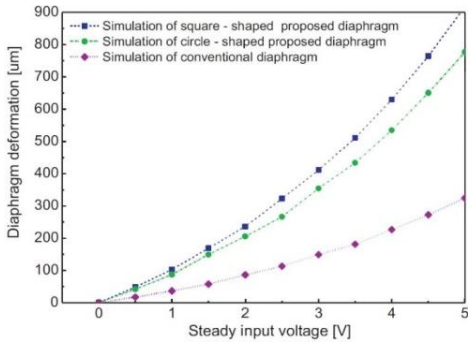

Fig. 10: Input voltage vs. displacement.

CONCLUSION

Nowadays the technology of producing biological fibers by 3D printers is rapidly developing. Increasing the efficiency of these printers would be a great step in this path. In this paper, the function of micro pump diaphragm especially IPMC actuators was explained. This diaphragm is one of the most important segments of the 3D biological printers. The simulating proses has been done by Abaqus and finally triangular form of IPMC actuators are proposed which have more efficiency and have more deformation capacity compared to circular and conventional designs. It is also obvious that the square-shape diaphragm is totally more effective than the circular one, if 5 V is applied to the system, there will be 16.7 % higher displacement. In the other words, the displacement of square type is 900 µm and in the later one is about 750 µm.

DISCLOSURE STATEMENT

The author(s) did not report any potential conflict of interest.

REFERENCES

1. Ghani M, Soleimanimehr H, Shirani Bidabadi E. An investigation the effect of Acidithiobacillus ferrooxidans bacteria on biomachining of titanium alloy and copper. Journal of Modern Processes in Manufacturing and Production. 2020;9:25-32.
2. Hossein-Fakhrzade R I. “An introduction to biological printing as a new method in tissue engineering. Iran diabetes and Lipid Magezin. 2011.
3. Farshchi Yazdi SA, Corigliano A, Ardito R. 3-D design and simulation of a piezoelectric micropump. Micromachines. 2019;10:259.
4. Biniyazan F, Soleimanimehr H. Improving both strength and ductility of Al-7075 by combining dual equal channel lateral extrusion with aging heat treatment. Iranian Journal of Science and Technology, Transactions of Mechanical Engineering. 2021; in press.
5. Soleimanimehr H, Nategh MJ, Najafabadi AF, Zarnani A. The analysis of the Timoshenko transverse vibrations of workpiece in the ultrasonic vibration-assisted turning process and investigation of the machining error caused by this vibration. Precision Engineering. 2018;54:99-106.
6. Soleimanimehr H. Analysis of the cutting ratio and investigating its influence on the workpiece’s diametrical error in ultrasonic-vibration assisted turning. Proceedings of the Institution of Mechanical Engineers B. 2021;235:640-649.
7. Soleimanimehr H, Hosseini Z, Habibi M, Goortani BM. Energy harvesting from wind by piezoelectric for autonomous remote sensor. Advanced Journal of Science and Engineering. 2020;1:80-85.
8. Mohith S, Karanth PN, Kulkarni SM. Recent trends in mechanical micropumps and their applications: a review. Mechatronics. 2019;60:34-55.
9. Truong DQ, Ahn KK, Nam DN, Yoon JI. Identification of a nonlinear black-box model for a self-sensing polymer metal composite actuator. Smart Materials and Structures. 2010;19:085015.
10. Haq M, Gang Z. Ionic polymer–metal composite applications. Emerging Materials Research. 2016;5:153-164.
11. Almomani A, Hong W, Hong W, Montazami R. Influence of temperature on the electromechanical properties of ionic liquid-doped ionic polymer-metal composite actuators. Polymers. 2017;9:358.

12. Chaudhari SV, Chakrabarti MA. Modeling of concrete for nonlinear analysis using finite element code ABAQUS. International Journal of Computer Applications. 2012;44:14-18.
13. Mirzaei M. Making sense the ideas in silico. Lab-in-Silico. 2020;1:31-32.
14. Mirzaei M. Science and engineering in silico. Advanced Journal of Science and Engineering. 2020;1:1-2.
15. Soleimanimehr H, Mirzaei M. An introduction to lab-in-silico. Lab-in-Silico. 2021;2:1-2.
16. Zolfagharian A, Kouzani AZ, Khoo SY, Moghadam AA, Gibson I, Kaynak A. Evolution of 3D printed soft actuators. Sensors and Actuators A. 2016;250:258-272.
17. Nisar A, Afzulpurkar N, Mahaisavariya B, Tuantranont A. MEMS-based micropumps in drug delivery and biomedical applications. Sensors and Actuators B. 2008;130:917-942.
18. Bar-Cohen Y, Bao X, Sherrit S, Lih SS. Characterization of the electromechanical properties of ionomeric polymer-metal composite (IPMC). Smart Structures and Materials. 2002;4695:286-293.
19. Chen Z, Tan X. A control-oriented and physics-based model for ionic polymer-metal composite actuators. IEEE/ASME Transactions on Mechatronics. 2008;13:519-529.
20. Chen Z, Hedgepeth DR, Tan X. A nonlinear, control-oriented model for ionic polymer-metal composite actuators. Smart Materials and Structures. 2009;18:055008.
21. Nemat-Nasser S, Li JY. Electromechanical response of ionic polymer-metal composites. Journal of Applied Physics. 2000;87:3321-3331.
22. Nemat-Nasser S. Micromechanics of actuation of ionic polymer-metal composites. Journal of applied Physics. 2002;92:2899-2915.

Please visit the journal homepage:
https://adv-j-sci-eng.com